Journal of Magnetic Resonance **140,** 432–441 (1999)
Article ID jmre.1999.1863, available online at http://www.idealibrary.com on IDEAL®

^{1}H NMR Imaging of Residual Dipolar Couplings in Cross-Linked Elastomers: Dipolar-Encoded Longitudinal Magnetization, Double-Quantum, and Triple-Quantum Filters

M. Schneider, D. E. Demco, and B. Blümich[1]

Institut für Technische Chemie und Makromolekulare Chemie, Rheinisch-Westfälische Technische Hochschule, Worringerweg 1, D-52056 Aachen, Germany

Received December 21, 1998; revised June 29, 1999

Contrast filters for NMR imaging of residual ^{1}H dipolar couplings of elastomers are introduced based on dipolar-encoded longitudinal magnetization, as well as double- and triple-quantum coherences. The spin response is discussed in the initial excitation time regime for methylene, methyl, and methine protons applicable to poly(isoprene) and other elastomers, taking into account the hierarchy of dipolar couplings and the associated editing features of multiple-quantum experiments. The efficiency of these filters is investigated for a series of cross-linked poly(isoprene) samples. Spatially resolved dipolar-encoded longitudinal magnetization decays and double-quantum and triple-quantum buildup curves are presented for a phantom made of poly(isoprene) with different cross-link densities. Two-dimensional images representing residual dipolar couplings are presented using dipolar-encoded longitudinal magnetization, double-quantum, and triple-quantum contrast filters. Images from dipolar-encoded longitudinal magnetization and triple-quantum coherences show the highest resolution and contrast, respectively.

INTRODUCTION

In recent years magnetic resonance imaging has become a routine method in medical diagnostics (*1*). At the same time, the potential of this technique in addressing problems in a wide area of different fields, such as material science, polymers, petrochemicals, plants, and agriculture, has been realized (*2–4*). A number of different techniques, such as magic-echo phase encoding, multiple-pulse line narrowing, magic-angle spinning, and stray field imaging, have recently been reviewed (*5–8*, and references therein). Many of these techniques have been developed for imaging of solid polymers. The necessity for the use of such demanding techniques arises from the large linewidths of ^{1}H in these materials. In contrast, elastomers permit the application of conventional liquid-state imaging techniques due to their reduced static linewidths resulting from a combination of high segmental mobility and mostly zero crystallinity. Diverse applications of NMR imaging in elastomers have appeared in the literature. Topics addressed are phase separation (*9*), selective determination of component distribution in multicomponent systems (*10*), aging (*9, 11, 12*), biodegradation (*13*), water uptake (*14, 15*), morphology and defects (*16, 17*), filler distribution (*18*), homogeneity of cross-link density (*19–21*), and stress-induced effects (*22–25*).

Multiple-quantum (MQ) coherences, especially double-quantum (DQ) coherences of ^{1}H in dipolar-coupled systems, have been explored recently for investigation of residual dipolar couplings in elastomers like poly(styrene-co-butadiene) (*26*) and poly(isoprene) (*27*). When measured selectively for a given chemical structure these couplings can be correlated with the cross-link densities distribution. Moreover, the quadrupolar interaction of deuterated poly(butadiene) oligomers incorporated into elastic rubber bands was used to generate contrast in ^{2}H NMR images of local strain in stretched elastomers (*24, 25*). Furthermore, proton as well as deuterium DQ-filtered NMR imaging has been applied to map molecular order in biological tissues (*28, 29*).

The goal of this paper is to introduce new ^{1}H NMR contrast filters to select signals from residual dipolar couplings of segmental protons in elastomers. The filters are based on the decay of dipolar-encoded longitudinal magnetization and the buildup of MQ coherences. With reference to two-dimensional (2D) MQ NMR spectroscopy (*30, 31*) the methods reported below exploit the short-time regime of MQ excitation and reconversion periods. The possibility of MQ editing of different functional groups based on the hierarchy of dipolar couplings is discussed. Parameter images of ^{1}H residual dipolar couplings can be recorded and correlated with spatial variations in cross-link density of elastomers.

THEORY

Depending on the type and the timescale of the NMR experiment the existence of an extended proton dipolar network along the polymer chain can be shown. Recently, ^{1}H DQ high-resolution MAS spectra were recorded for poly(styrene-co-butadiene), using recoupling pulse sequences with long excitation times (*26*). These spectra directly show the existence

[1] To whom correspondence should be addressed.

1090-7807/99 $30.00

of dipolar connectivities between *all* functional groups. The existence of such a network was also demonstrated by NOESY spectra recorded for long mixing times (*32*). Nevertheless, if the integral intensities of diagonal peaks are compared with those of cross peaks all these experiments also show the existence of a strong *hierarchy* of the dipolar couplings. Further theoretical and experimental support for the existence of a strong coupling hierarchy was given for poly(isoprene) by a ^{1}H DQ MAS spectrum recorded with a three-pulse sequence (*27*).

One of the important features of MQ spectroscopy is the possibility to *edit* the strongest dipolar couplings. This feature is based on the fact that the efficiency of MQ pumping is a nonlinear function of the dipolar coupling strength. For instance, in the *initial* excitation time regime the pumping efficiencies for DQ and TQ coherences are proportional to $(D^{ij})^2$ and $(D^{ij})^4$, respectively, where D^{ij} is the strength of the dipolar coupling between protons i and j (*33–35*). Therefore, one can estimate that the pumping efficiency of DQ coherences for methylene protons is about six times higher than that of methyl protons. The difference in dipolar coupling strengths is expected to be even higher for intergroup dipolar interactions. In the case of TQ coherences the maximum pumping efficiency is expected for the methyl group (*35*).

In the following the spin system response of a dipolar network which generally is present in elastomers and polymer melts is discussed. The density matrix formalism is employed. The sample is static, i.e., nonspinning. As an example cross-linked poly(isoprene) is considered, which provides dipolar-coupled methine, methylene, and methyl protons. But the results can be extended to other elastomers and polymer melts as well. The pulse sequences employed are presented in Fig. 1. They consist of an excitation, an evolution, a reconversion, and a detection period (Fig. 1a) (*30*). In this work the classical three-pulse sequence (*30*) fitted with 180° refocusing pulses in the middle of excitation and reconversion periods is used for excitation of double- and triple-quantum coherences as well as dipolar-encoded longitudinal magnetization (Figs. 1b and 1c).

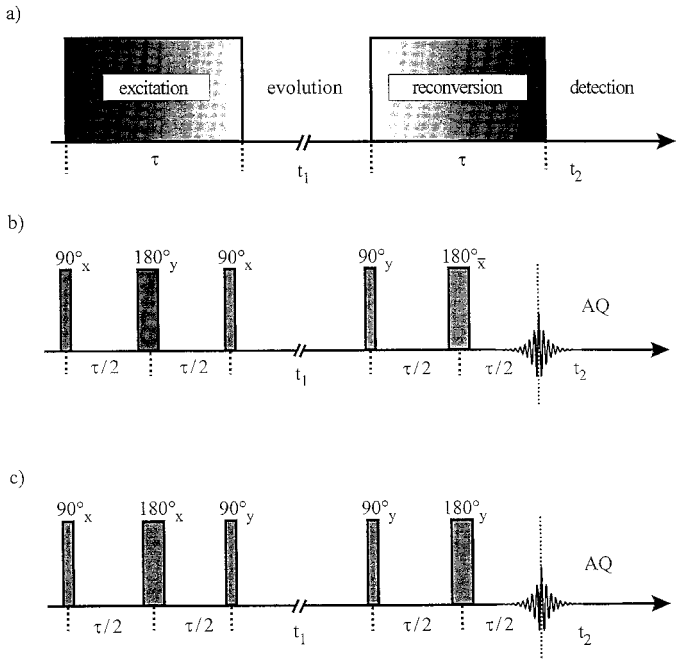

FIG. 1. (a) Schematic representation of the experiment for excitation of dipolar-encoded longitudinal magnetization and multiple-quantum coherences. This scheme is similar to that for two-dimensional MQ spectroscopy but it is used with fixed evolution time t_1 for recording dipolar-encoded longitudinal magnetization decays and DQ and TQ buildup curves. (b) The three-pulse sequence supplemented by 180° refocusing pulses for measuring dipolar-encoded longitudinal magnetization and DQ-filtered magnetization with variable excitation and reconversion times τ. The phase cycles used are different for longitudinal magnetization and DQ experiments. (c) The three-pulse sequence supplemented with 180° refocusing pulses for TQ coherence experiments with variable excitation and reconversion times τ.

Dipolar-Encoded Longitudinal Magnetization

Longitudinal magnetization (LM) can be excited by the three-pulse sequence presented in Fig. 1b in combination with phase cycling similar to that used for selection of zero-quantum coherence (*30, 31*). In this case the periods of duration τ are called dipolar encoding periods. The density operator formalism can be used to evaluate the longitudinal magnetizations from CH, CH_2, and CH_3 protons at the end of the exitation/reconversion pulse sequence (cf. Fig. 1b) for a static sample. The existence of this longitudinal magnetization was also evidenced for spin pairs $\frac{1}{2}$ under magic-angle sample spinning conditions (*34*). The normalized, integral NMR signal detected by half of the dipolar echo in the t_2 dimension of the experiment is given by (*27*)

$$S_{\mathrm{LM}}(\tau + t_1 + \tau;\, t_2 = 0) \approx \frac{1}{8} + \frac{1}{2}\left\langle\left\langle \cos^2\left[\sqrt{\frac{3}{2}}\,\bar{\omega}_{\mathrm{d}}^{(2)}\tau\right]\right\rangle\right\rangle + \frac{3}{8}\left\langle\left\langle\left[\frac{3}{5}\cos[\sqrt{6}\,\bar{\omega}_{\mathrm{d}}^{(3)}\tau] + \frac{2}{5}\right]^2\right\rangle\right\rangle. \qquad [1]$$

The first term in the right-hand side describes the longitudinal magnetization of the CH group which, in the regime of short excitation times, is not affected by intergroup dipolar couplings. The second and the third terms are for the methylene and methyl groups of poly(isoprene), respectively. The signal in the orthogonal channel has negligible intensity for close-to-resonance irradiation. Any relaxation of coherences during dipolar encoding and evolution periods as well as the longitudinal relaxation is neglected. Furthermore, the intergroup residual dipolar couplings are neglected in the equation above because of their much weaker contribution to the total signal. Nevertheless, even in the short dipolar encoding regime the presence of the *full* dipolar network can be taken into account (see below).

An *enhanced* effect of the dipolar interactions as compared to the free induction decay is present in the signal from dipolar-encoded longitudinal magnetization recorded with the pulse sequence of Fig. 1b. If n such periods are applied during the lifetime of the free induction decay the response is similar to that given by Eq. [1], but with the exponents of two of the last two terms replaced by n.

The residual dipolar couplings of methylene and methyl protons contained in Eq. [1] are given by (see, for instance, Refs. (*26, 27*))

$$\bar{\omega}_{\mathrm{d}}^{(2)} = \frac{(-\sqrt{6})}{2} D^{(2)} S^{(2)} \frac{k}{N^2 a^2} \mathbf{R}^2 P_2(\cos\beta) \qquad [2]$$

and

$$\bar{\omega}_{\mathrm{d}}^{(3)} = \frac{(-\sqrt{6})}{4} D^{(3)} S^{(3)} \frac{k}{N^2 a^2} \mathbf{R}^2 P_2(\cos\beta), \qquad [3]$$

respectively. The dipolar coupling constant $D^{(2)} = (\mu_0/4\pi)\gamma^2\hbar(1/r_{ij}^3)$ of the spin pairs ij depends on the internuclear distance r_{ij}. For methyl groups the dipolar coupling constant is given by $D^{(3)} = (\mu_0/4\pi)\gamma^2\hbar(1/r^3)$, where r is the distance between the methyl protons ($r = 0.19$ nm).

The dynamic order parameter is given by $S^{(2)} \equiv \bar{P}_2[\cos\theta^{ij}(t)]$, where $\theta^{ij}(t)$ is the instantaneous angle between a given internuclear vector $\mathbf{r}_{ij}$ and the end-to-end vector $\mathbf{R}$, i.e., the vector connecting two neighboring cross-link junctions (*36*). The bar in Eqs. [2] and [3] and in the above definition of dynamic order parameter represents the time average over the molecular reorientation which is faster than the spin-precession period in the local dipolar field of the rigid lattice. This averaging by rapid segmental motions is referred to as "preaveraging" (*37*). The angle between $\mathbf{R}$ and $\mathbf{B}_0$ is denoted by β. The geometrical factor k depends on the model which is adopted to describe the chain statistics and is equal to $\frac{3}{5}$ for a chain of freely jointed segments (*36*). The methyl order parameter $S^{(3)}$ is given by the average of the second-order Legendre polynomial the argument of which contains the cosine of the angle between the instantaneous orientation of the C_3 axis and the end-to-end vector $\mathbf{R}$. In a disordered polymer, the end-to-end vector is assumed to obey Gaussian statistics (*37*). The statistical average (denoted by $\langle(\cdots)\rangle_R$) of the squared end-to-end vector is given by $\langle\mathbf{R}^2\rangle_R \approx Na^2$, where a is the length of a statistical segment and N is the number of the statistical segments. Thus, the averaged residual dipolar couplings given by Eqs. [2] and [3] scales with N^{-1}. In Eq. [1], the symbol $\langle\langle\ \rangle\rangle \equiv \langle\langle\ \rangle_\Omega\rangle_R$ represents the ensemble average over the distribution of end-to-end vectors and the powder average of the angular part of the residual dipolar coupling in the disordered elastomer.

For short encoding times, i.e., $\tau\|\bar{H}_{\mathrm{d}}^{(g)}\| \ll 1$, where $g = 2$, 3 and $\|\bar{H}_{\mathrm{d}}^{(g)}\|$ is the norm of the residual dipolar Hamiltonian, the integral signal intensity of the normalized LM decay can be evaluated from Eq. [1],

$$\begin{aligned} S_{\mathrm{LM}}(\tau + t_1 + \tau;\, t_2 = 0) &\approx 1 - \{l_2[D^{(2)}S_{\mathrm{s}}^{(2)}]^2 + l_3[D^{(3)}S_{\mathrm{s}}^{(3)}]^2 \\ &\quad + [\text{intergroup } DS]^2\}\tau^2 - \cdots \\ &\equiv 1 - [D_{\mathrm{eff}}^{\mathrm{LM}}]^2\tau^2 - \cdots, \end{aligned} \qquad [4]$$

where the numerical coefficients are $l_2 = 21/80$ and $l_3 = 63/190$. $D_{\mathrm{eff}}^{\mathrm{LM}}$ is the effective residual dipolar coupling describing contributions from intergroup residual dipolar couplings of the CH, CH_2, and CH_3 groups. Nevertheless, the residual dipolar couplings of methylene and methyl protons dominate the intergroup couplings (*27*) and the slope of the LM decay curve versus the square of the excitation time τ gives access to a weighted sum of squares of dynamic order parameters of methylene and methyl groups.

Double-Quantum Buildup Signal

The normalized, integral DQ NMR signal detected by half of the dipolar echo in the t_2 dimension of the experiment presented in Fig. 1b can be evaluated in the same manner as the LM signal. For a short evolution time t_1 the DQ signals originating from the CH_2 and CH_3 groups are given by (for the details of the evaluation see Refs. (*27, 34, 35*))

$$\begin{aligned} S_{\mathrm{DQ}}(2\tau;\, t_2 = 0) &\approx \frac{1}{2}\left\langle\left\langle \sin^2\left[\sqrt{\frac{3}{2}}\,\bar{\omega}_{\mathrm{d}}^{(2)}\tau\right]\right\rangle\right\rangle \\ &\quad + \frac{3}{10}\langle\langle\sin^2[\sqrt{6}\,\bar{\omega}_{\mathrm{d}}^{(3)}\tau]\rangle\rangle. \end{aligned} \qquad [5]$$

In the limit of a short excitation time, i.e., for $\bar{\omega}_{\mathrm{d}}^{(g)}\tau \ll 1$ with $g = 2$, 3, the DQ signal can be evaluated from Eq. [5], and one can finally write

$$\begin{aligned} S_{\mathrm{DQ}}(2\tau;\, t_2 = 0) &\approx \{d_2[D^{(2)}S_{\mathrm{s}}^{(2)}]^2 + d_3[D^{(3)}S_{\mathrm{s}}^{(3)}]^2 \\ &\quad + [\text{intergroup } DS]^2\}\tau^2 - \cdots \\ &\equiv [D_{\mathrm{eff}}^{\mathrm{DQ}}]^2\tau^2 - \cdots, \end{aligned} \qquad [6]$$

where the numerical coefficients are $d_2 = 21/40$ and $d_3 = 9/200$. An effective residual dipolar coupling $D_{\mathrm{eff}}^{(\mathrm{DQ})}$ can be introduced describing *all* the active residual dipolar coupling. This effective coupling is not identical with $D_{\mathrm{eff}}^{(\mathrm{LM})}$, because the dipolar network is edited differently by these experiments. The relative contributions of the two more intense DQ coherences can be estimated for the *initial* excitation time regime considering that $S_{\mathrm{s}}^{(2)} \approx S_{\mathrm{s}}^{(3)}$ (*27*), and that the interproton distances of methylene and methyl groups are 0.18 and 0.19 nm, respectively. One obtains the ratio $(d_3/d_2)(D^{(3)}/D^{(2)})^2 \approx 0.08$; i.e.,

the contribution from the methyl protons to the total DQ signal detected is estimated from theory from this excitation time regime to be in the order of 8%. Hence, in a good approximation the DQ buildup gives direct access to the dynamic order parameter of the CH_2 groups in the short-time regime.

Triple-Quantum Buildup Signal

Triple-quantum coherences can be excited starting from initial z magnetization using the sequence depicted in Fig. 1c. In the regime of short excitation times the TQ coherences are derived mainly from the methyl protons.

For this pulse sequence the spin response of a proton triad rapidly rotating around the C_3 axis in a static sample can be evaluated similar to that of DQ coherences (*35*). The TQ coherence is a total spin coherence in the approximation of the isolated methyl group and does not evolve during the evolution period t_1. Nevertheless, the dipolar couplings with the passive methyl proton as well as the remote protons affect the lifetime of these coherences (*35*). These effects can be neglected for short evolution times t_1. The normalized TQ signal can be finally written as (*27*)

$$S_{\mathrm{TQ}}(2\tau;\, t_2 = 0) \approx \frac{27}{320} \langle\langle [\cos[\sqrt{6}\ \bar{\omega}_{\mathrm{d}}^{(3)}\tau] - 1]^2 \rangle\rangle. \quad [7]$$

The normalization is taken with respect to the total integral intensity of the ^{1}H NMR spectrum. In the limit of short excitation times the TQ filtered signal is given by

$$\begin{aligned} S_{\mathrm{TQ}}(2\tau;\, t_2 = 0) &\approx \{r_3[D^{(3)}S_{\mathrm{s}}^{(3)}]^4 + [\text{intergroup } DS]^4\}\tau^4 - \cdots \\ &\equiv [D_{\mathrm{eff}}^{\mathrm{TQ}}]^4\tau^4 - \cdots, \end{aligned} \quad [8]$$

where $r_3 = 39/4$. An effective residual dipolar coupling $D_{\mathrm{eff}}^{(\mathrm{TQ})}$ can be introduced for the full dipolar network. It is expected to be dominated by the TQ coherences of the methyl protons. In this approximation, the dynamic order parameter of the methyl group can be estimated from the normalized TQ buildup intensities.

In order to describe the τ dependence of the detected signals relaxation has to be considered for the single-quantum coherences as well as for the MQ coherences and the dipolar-encoded LM in all periods of the experiment (cf. Fig. 1a). For instance, transverse relaxation has been taken into account by multiplying the detected signal with a global relaxation function $\exp\{-2\tau/\bar{T}_2\}$, where $\bar{T}_2$ is the average transverse relaxation time of the SQ coherences.

TABLE 1

Series of Cross-Linked Synthetic Poly(isoprene) Samples and Effective Residual Dipolar Couplings Extracted from the Short-Time Regime of LM Decay Curves and DQ and TQ Buildup Curves

Sample	DICUP content (phr)	$D_{\mathrm{eff}}^{\mathrm{LM}}$ (Hz)[a]	$D_{\mathrm{eff}}^{\mathrm{DQ}}$ (Hz)[b]	$D_{\mathrm{eff}}^{\mathrm{TQ}}$ (Hz)[b]
A	0.75	307	257	120
B	3.75	356	349	155
C	7.5	547	1412	220

[a] Uncertainties are ≤10%.
[b] Uncertainties are ≤20%.

EXPERIMENTAL

Samples and Phantom

The elastomer system investigated is based on commercially available synthetic 1,4-*cis*-poly(isoprene). According to the specifications of the manufacturer this elastomer has a molecular weight $M_{\mathrm{w}} \approx 952\,110$ g/mol (GPC–gel permeation chromatography) and a molecular weight distribution $M_{\mathrm{w}}/M_{\mathrm{n}} = 4.35$. The repetition units were 97.5% *cis*-1,4-isoprene and 2.5% 3,4-isoprene. The glass transition temperature T_{g} is about 210 K. Cross-linking was achieved by a radical mechanism. The initiator system consisted of 40% dicumylperoxid (DCP) on kaolin as a carrier material (DICUP). The amounts of DICUP for individual poly(isoprene) samples in the cross-link series are listed in Table 1. The samples were vulcanized at 150°C until 90% of the maximum torque was achieved on the rheometer curve for the respective sample.

The phantom used for spatially resolved one-dimensional (1D) decay and buildup curves and parameter 2D images was made from cylindrical poly(isoprene) samples separated by Teflon spacers in the order B-C-A, where A, B, and C are the samples defined in Table 1. The phantom diameter is about 15 mm and the thickness of samples and spacers is 4 and 1 mm, respectively.

NMR Experiments

The NMR measurements were performed at a ^{1}H frequency of 200.085 MHz on a Bruker DSX-200 spectrometer using a microimaging probe. The measurements were done at room temperature ($T = 293$ K), which corresponds to $T \approx T_{\mathrm{g}} + 80$ K for the elastomers investigated. The dipolar-encoded LM decays and DQ buildup intensities were recorded with the pulse sequence in Fig. 1b. It is based on the general scheme (cf. Fig. 1a) of MQ 2D NMR spectroscopy (*30, 31*). The 180° radiofrequency pulses refocus the chemical shielding interaction as well as the spin interaction with the magnetic field inhomogeneities. For filtering SQ and MQ coherences phase cycling was used in combination with CYCLOPS. In the experiments using longitudinal magnetization T_1 relaxation

was neglected. The TQ coherence buildup intensities were measured using the same pulse sequence as in Fig. 1b but with a 90° phase shift of the last 90° pulse in the excitation period (Fig. 1c). In order to support DQ and TQ editing the irradiation frequency was set at the resonance frequencies of methylene protons and methyl protons in the respective experiments. Moreover, DQ and TQ buildup curves were recorded separately for each sample by taking the integral intensities of the absorption NMR spectra around the CH_2 and CH_3 resonances, respectively.

The 90° pulse length for investigations of contrast filter efficiency and image acquisitions was 2.52 and 33 μs, respectively. A recycle delays of 1.5 s was used in all experiments. The evolution time was fixed to $t_1 = 10$ ms and $t_1 = 100$ μs in the experiments for measuring LM decays and DQ buildup intensities. In order to avoid relaxation of TQ coherences the duration of the evolution time t_1 was reduced to 50 μs. In all experiments the excitation and reconversion times were varied in the range from 2 μs to 2.3 ms.

Transverse magnetization decays encoded by both residual dipolar interactions as well as molecular motions were recorded using the Hahn-echo pulse sequence (*2*). This pulse sequence was applied for variable delays between excitation and refocusing pulses in the range from 5 μs to 8 ms, and the integral intensities derived from the Fourier transform of the full Hahn echoes were used as data entries.

1D spatially resolved ^{1}H filter curves were recorded with a pulse sequence which combines the pulse sequences used for dipolar-encoded LM decays and DQ and TQ buildup curves (cf. Figs. 1b and 1c) with imaging by frequency encoding based on the Hahn spin echo (see below). For 2D parameter images a phase-and-frequency encoding procedure was used (*2*). The microimaging unit consisted of a homebuilt gradient coil system. In all images the spatial resolution was about 300 μm in both directions with a field of view of about $(20\ \text{mm})^2$. The maximum achievable gradient strength was approximately 93 mT/m. The gradient was stepped through 64 gradient values. For parameter and spin-echo images the space encoding τ_i time (see below) was 0.8 ms. The total duration for acquisition of 2D filtered images was on the order of 5 h.

RESULTS AND DISCUSSION

Filter Efficiency

MQ editing of the different functional groups can be demonstrated by recording ^{1}H MQ-filtered spectra. In Fig. 2 the 300-MHz ^{1}H NMR spectrum is presented for the static poly(isoprene) A sample of Table 1. The spectrum is not resolved but is approximately symmetric except for a shoulder corresponding to the —CH═ resonance positioned at about 3.3 ppm off center from the main peak. For 1,4-*cis*-poly(isoprene) (latex) the corresponding high-resolution spectrum in solution shows four lines: one at 5.2 ppm (relative to HMDS) for —CH═, two lines at 2.2 and 2.15 ppm for —CH_2—, and one at 1.75 ppm corresponding to –CH_3 functional groups. However, for all samples from our cross-link series of synthetic poly(isoprene) the CH_2 and CH_3 resonances, separated by about 0.5 ppm, are not resolved for the static samples.

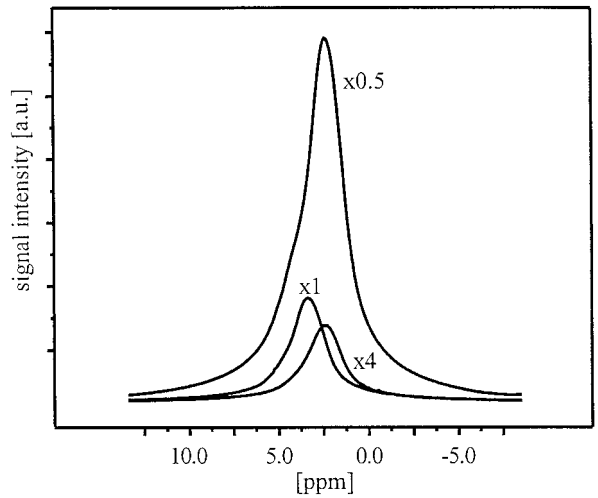

FIG. 2. DQ (×1)- and TQ (×4)-filtered ^{1}H NMR spectra in the regime of short excitation and reconversion times ($\tau = 50$ μs) and the ^{1}H NMR spectrum (×0.5) recorded for synthetic poly(isoprene) (sample A in Table 1).

Proton DQ- and TQ-edited spectra are also presented in Fig. 2. The MQ-filtered spectra were recorded using the pulse sequence of Fig. 1b for DQ and of Fig. 1c for TQ coherences with a fixed evolution time t_1 of 100 μs and short excitation-and-reconversion times $\tau = 50$ μs. The integral intensities of the spectra are normalized to the DQ-edited spectrum (×1, in Fig. 2). The static ^{1}H spectrum (×0.5) and TQ-edited spectrum (×4) are also shown in Fig. 2. It is evident that the relative intensity of the signals follows the expected dependence given by Eqs. [5] and [7]. The DQ-filtered signal is centered close to the CH_2 resonance. The TQ-filtered signal is also centered in the vicinity of the methyl resonance. Both spectra are symmetric to a high degree. Nevertheless, the separation of the peaks is slighter larger than the expected 0.5 ppm. These results prove that in the regime of short excitation times the DQ coherences are excited mainly from the strongest dipolar-coupled protons, i.e., from methylene groups. Nevertheless, DQ coherences corresponding to the intergroup protons belonging to CH, CH_2, and CH_3 groups as well as from protons within CH_3 groups are excited to a smaller degree, as evidenced by the wings of the DQ-filtered spectrum in the region of these resonances. For an increased excitation-and-reconversion time of $\tau = 1.5$ ms the DQ- as well as TQ-filtered spectra (not shown) are broader with the more pronounced wings in the neighboring regions showing delocalized pumping of DQ and TQ coherences.

In order to characterize the filter efficiency dipolar-encoded LM decay curves were measured for a series of cross-linked synthetic poly(isoprene) samples. The decays for three samples

with cross-link densities (Table 1) are shown in Fig. 3a for relevant values of the excitation time τ. The LM decays are encoded by the intra- and intergroup dipolar couplings as well as by transverse relaxation during dipolar encoding times. They are sensitive to cross-link density. In the short-time regime the dipolar-encoded LM decays show a linear dependence in τ^2, in accordance with Eq. [4]. For longer dipolar encoding times a deviation from this dependence arises which is more pronounced as cross-linked density increases. The recorded signals exhibit good signal-to-noise ratio and permit extraction of the effective residual dipolar couplings $D_{\text{eff}}^{\text{LM}}$ (cf. Eq. [4]) from the τ^2 dependence of the decay curves. These effective couplings characterizing the full dipolar network are listed in Table 1. The sensitivity of LM decays to residual dipolar couplings in the limit of short encoding times is higher than that of DQ and TQ buildup curves due to contributions from all functional groups.

DQ buildup curves for the same samples have been measured for the full range of excitation times τ and are shown in Fig. 3b. The maxima of the DQ signals arise from (i) the transverse relaxation during excitation and reconversion times and (ii) the excitation of high-order MQ coherences in the dipolar network of coupled protons. The first process is dominant in elastomers. The systematic dependence of the DQ-filtered signal intensity on the excitation time τ can be exploited for generation of contrast in imaging of differently cross-linked elastomers. The effective dipolar couplings $D_{\text{eff}}^{\text{DQ}}$ can be evaluated from these DQ buildup curves by fitting the curves with a polynomial in τ^2. The values of $D_{\text{eff}}^{\text{DQ}}$ obtained in this way are collected in Table 1.

TQ buildup curves for characterization of the efficiency of a contrast filter based on residual dipolar couplings are shown in Fig. 3c. A clear dependence of the curves on the cross-link density is found similar to the case of the DQ buildup curves. Effective residual dipolar couplings $D_{\text{eff}}^{\text{TQ}}$ were obtained by fitting the data in the initial time regime by a polynomial in τ^4 (see Eq. [8]). The values of $D_{\text{eff}}^{\text{TQ}}$ for the samples of the cross-link series are collected in Table 1. In all of these as well as in other cases (*27*) the measured residual dipolar couplings show a linear proportionality to the cross-link density in good approximation.

The results above demonstrate that contrast filters based on residual dipolar couplings can be implemented using dipolar-encoded LM decays and DQ and TQ coherence buildup. The LM decays are expected to provide the highest signal-to-noise ratio and consequently the highest resolution in NMR imaging. The residual dipolar coupling contrast for LM decays and DQ buildup curves in the excitation time regions marked by dashed lines in Figs. 3a and 3b is about the same. In region I (cf. Fig. 3b) the contrast is changing in the same direction as cross-link density. This is not the case for region II (cf. Fig. 3b) where the sign of the intensity differences has changed in one case so that the resultant image intensity cannot directly be correlated with the values of cross-link density. The highest contrast is offered

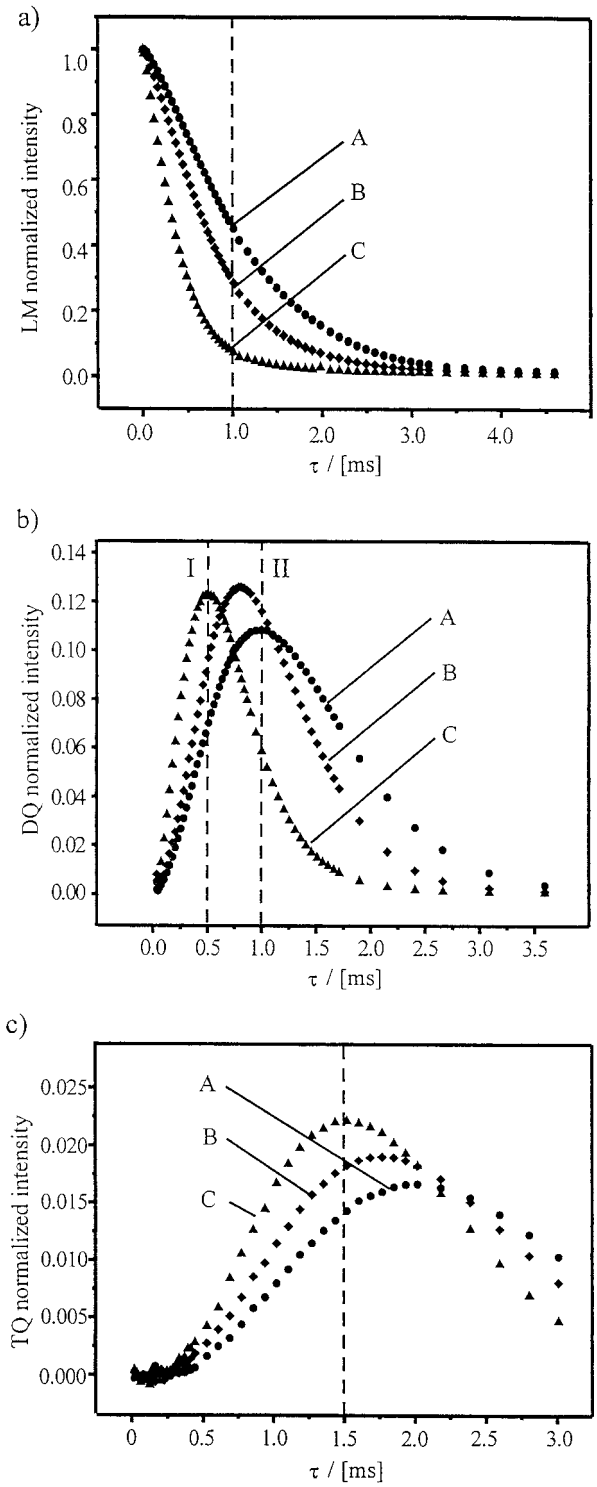

FIG. 3. (a) ^{1}H dipolar-encoded longitudinal magnetization decay curves recorded using the pulse sequence of Fig. 1b with a phase cycle for zero-quantum coherence. (b) ^{1}H DQ buildup curves recorded by the three-pulse sequence of Fig. 1b. (c) ^{1}H TQ buildup curves recorded by using the pulse sequence of Fig. 1c. The DQ and TQ signals are normalized to the integral intensity of the SQ NMR spectrum for each sample. A series of samples from synthetic poly(isoprene) with different cross-link densities (cf. Table 1) was investigated.

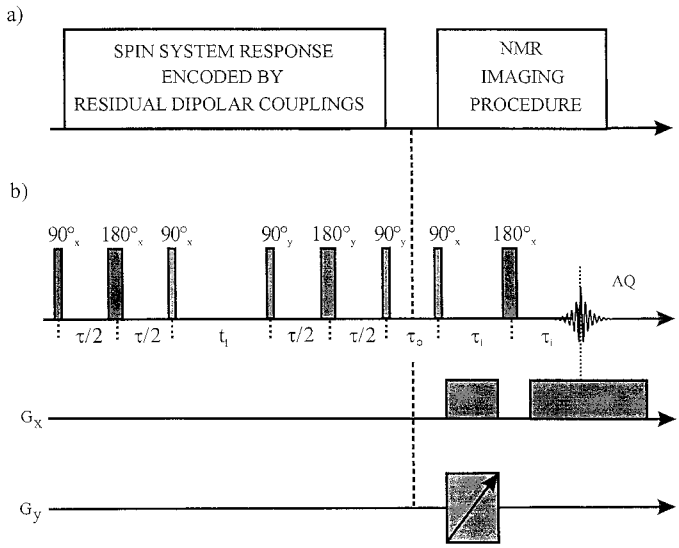

FIG. 4. (a) General scheme used for recording images weighted by residual dipolar couplings. (b) Three-pulse sequence with 180° refocusing pulses for filtering according to residual dipolar couplings followed by a *z* filter and space encoding by 2D spin-echo imaging.

by the TQ buildup curves. This can be understood by considering the initial excitation time regime where the buildup rates of TQ signals are proportional to $(D_{\mathrm{eff}}^{\mathrm{TQ}})^4$ compared to the DQ and LM filters where the rates are proportional with $(D_{\mathrm{eff}}^{\mathrm{DQ}})^2$ and $(D_{\mathrm{eff}}^{\mathrm{LQ}})^2$. Nevertheless, the signal-to-noise ratios for TQ signals are much weaker than those for LM and DQ signals. The sensitivity to the cross-link density is higher for dipolar-encoded LM and MQ signals compared to contrast from transverse relaxation only, because the LM and DQ filters include a transverse relaxation weight.

Images Weighted by Residual Dipolar Couplings

Spatially resolved ^{1}H LM decays, DQ and TQ buildup curves, and images encoded by residual dipolar couplings were recorded with the pulse sequence shown in Fig. 4. It has been used for experiments with 1D as well as 2D spatial resolution. The principle of the method is a classical combination of a spin response encoded by residual dipolar couplings and an NMR imaging technique for the generation of spatial resolution (cf. Fig. 4a) (*2*, *38*). The pulse sequences used for LM, DQ, and TQ filters (cf. Figs. 1b and 1c) have been modified by appending a final flip-back 90° pulse to the filters (cf. Fig. 4b). The subsequent dephasing period of duration τ_0 forms an additional *z* filter.

Dipolar-encoded LM decays and DQ and TQ buildup curves are shown at the top of Figs. 5 to 8 with 1D spatial resolution. To a good approximation they reproduce the curves measured on the individual samples of the poly(isoprene) cross-link series without space encoding (cf. Fig. 3). The middle and the bottom parts of Figs. 5 to 8 depict 2D ^{1}H NMR images obtained with LM, DQ, TQ, and T_2^* contrast filters, respectively. The highest contrast is observed for the images in the middle of each figure. This is related to the fact that the LM, DQ, and TQ contrast filters also include contrast weights from transverse relaxation. Because LM and T_2^* contrast filters are both based on signal decays the contrast from residual dipolar coupling in Fig. 5 is going in the same direction as the T_2^* contrast for any value of dipolar encoding times. The τ value recommended for maximum contrast by the LM filter is indicated by a dashed line in Fig. 3a. The contrast scale is inverted for DQ and TQ filters which use buildup curves. As expected, the highest contrast is shown for the TQ-filtered image (cf. Fig. 7). Nevertheless, the image has lower spatial resolution than the images presented in Figs. 5 and 6. The τ values chosen for excitation are indicated by the dashed line I in Fig. 3b and by the dashed line in Fig. 3c.

Parameter Images of Residual Dipolar Couplings

Parameter images of residual dipolar couplings in elastomer samples with spatially distributed cross-link density can be

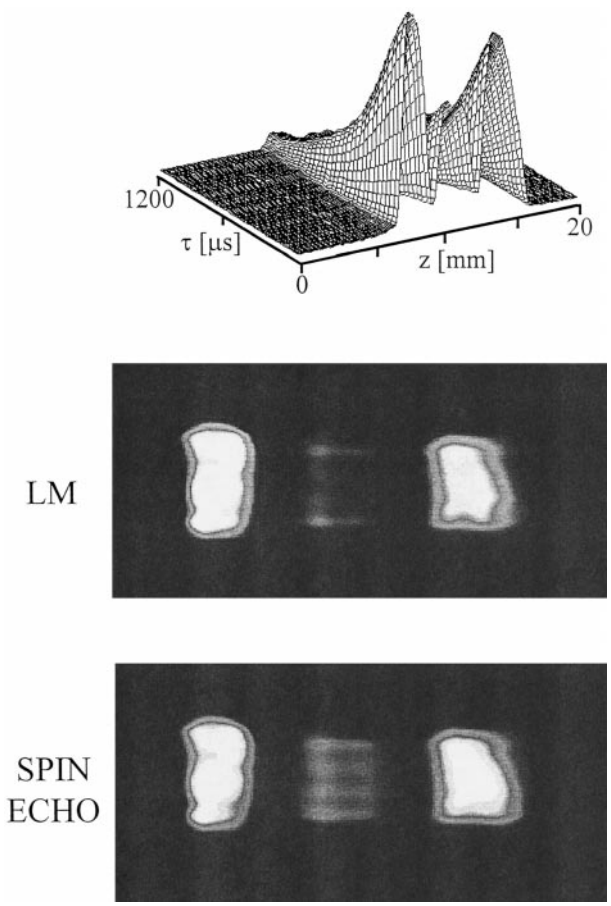

FIG. 5. Spatially resolved curves of dipolar-encoded LM decays (top). Two-dimensional images weighted by ^{1}H residual dipolar couplings using LM (middle) and a spin-echo image (bottom). From left to right the signals of the phantom correspond to samples B, C, and A (cf. Table 1), respectively. The data were recorded with the pulse sequence shown in Fig. 1b and Fig. 4b.

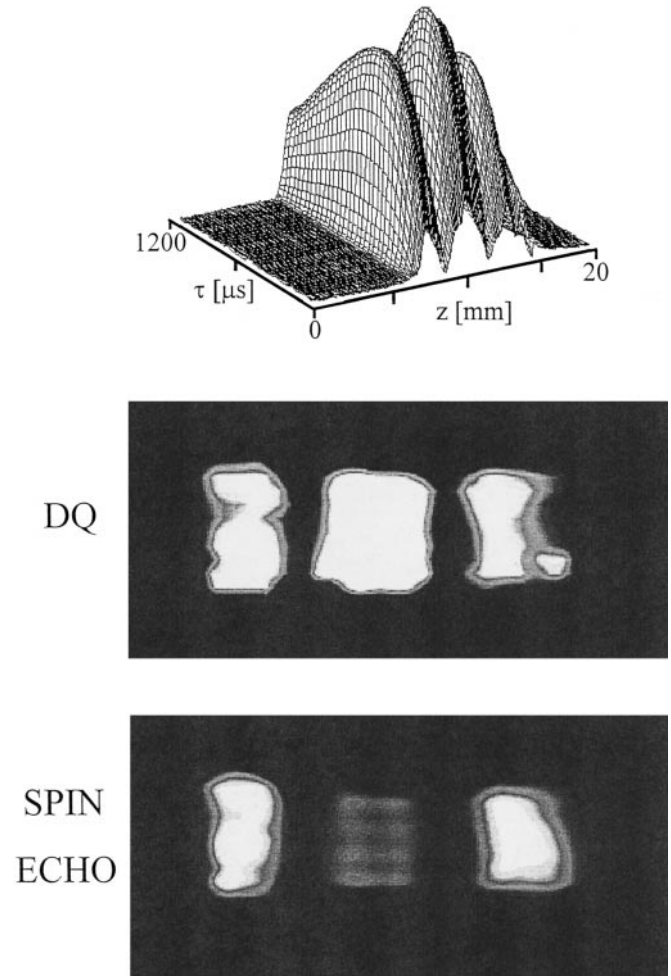

FIG. 6. Spatially resolved curves of dipolar-encoded DQ buildup (top). Two-dimensional images weighted by ^{1}H residual dipolar couplings using DQ coherences (middle) and a spin-echo image (bottom). From left to right the signals of the phantom correspond to samples B, C, and A (cf. Table 1), respectively. The data were measured with the pulse sequence shown in Fig. 1b and Fig. 4b.

obtained if several images are recorded with different excitation times. In order to eliminate spin density and transverse relaxation encoding a T_2^*-filtered image needs to be recorded as well. Each pixel of the LM- DQ- and TQ-filtered images recorded by the scheme presented in Fig. 4 has to be divided by the spin-echo image $\rho(\mathbf{r})R(2\tau)$, where $\rho(\mathbf{r})$ is the spatially distributed spin density and $R(2\tau)$ is the effective relaxation function which accounts for transverse relaxation in phase and frequency encoding. Proton parameter images of residual dipolar couplings of the elastomer phantom obtained in this way from the images of Figs. 5 to 7 are shown in Fig. 8. All the images now show less contrast because the effects of spin density and transverse relaxation are eliminated. The fact that the contrast differs in each image is attributed to the different excitation times τ, as a result of which the dipolar coupling hierarchy is probed on different length scales.

CONCLUSIONS

New residual dipolar coupling contrast filters based on dipolar-encoded longitudinal magnetization decay curves and DQ and TQ buildup curves of ^{1}H are introduced. They show different filtering efficiency versus cross-link density. The most sensitive is the TQ contrast filter as a result of the characteristic functional dependence of the filtered signal on the dipolar coupling. The highest signal-to-noise ratio is provided by the contrast filter for dipolar-encoded longitudinal magnetization. For all filters the contrast is enhanced by transverse relaxation during the excitation-and-reconversion periods. The pulse sequence used for these filters are based on the classical three-pulse sequence of multi-quantum NMR spectroscopy. The efficiency in pumping MQ coherences can be

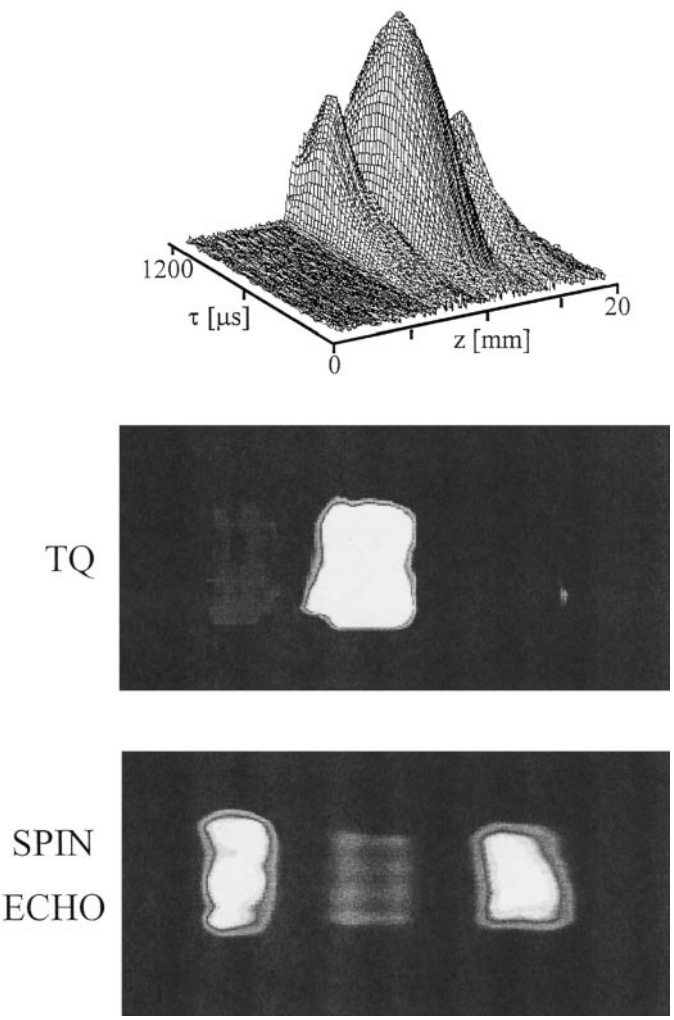

FIG. 7. Spatially resolved curves of dipolar-encoded TQ buildup (top). Two-dimensional images weighted by ^{1}H residual dipolar couplings using TQ coherences (middle) and a spin-echo image (bottom). From left to right the signals of the phantom correspond to samples B, C, and A (cf. Table 1), respectively. The data were measured with the pulse sequence shown in Fig. 1c and Fig. 4b.

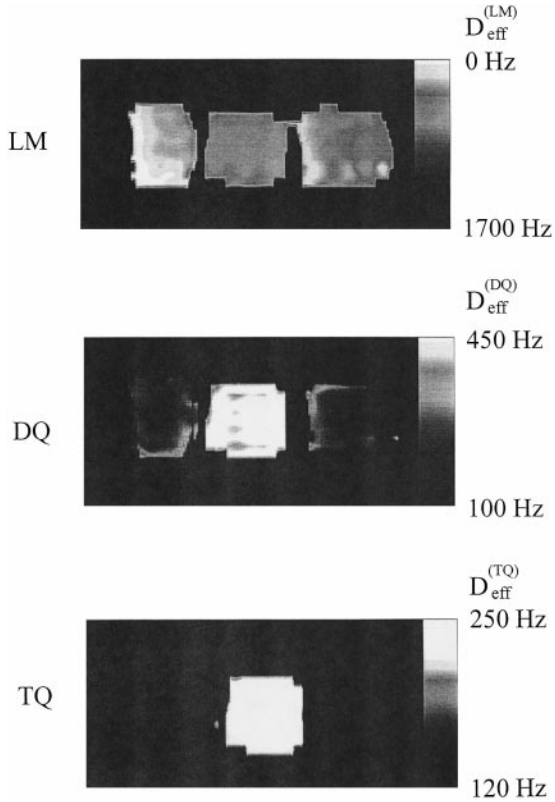

FIG. 8. Parameter images of ^{1}H residual dipolar couplings measured for the elastomer phantom using the LM, DQ, and TQ contrast filters shown in Fig. 4. These parameter images have been obtained by normalization of the images from Figs. 5 to 7 (middle) to the spin-echo image weighted by transverse relaxation (bottom in Figs. 5 to 7). For each image the scale of residual dipolar couplings is shown.

increased if, for instance, an eight-pulse sequence is used (*31*). Moreover, many dipolar encoding periods can be used for enhancing the effect of residual dipolar couplings on longitudinal magnetization decays.

Dipolar-encoded LM decays and DQ and TQ buildup curves were recorded for cross-linked elastomers with and without space encoding. The corresponding curves compare well with each other. Proton residual dipolar couplings can be measured with spatial resolution when exploring the initial time behavior of LM and MQ signals. In this time limit the MQ signals can be approximately assigned to specific chemical groups, so that signals can be edited by MQ filters based on the dipolar coupling strength. The values of residual dipolar couplings can be measured model free. This is not the case with other methods for recording material property images of cross-linked polymers (*20, 21*). These techniques are based on transverse relaxation and spin–lattice relaxation in the rotating frame and use models for the molecular dynamics of the polymer network. Nevertheless, MQ methods suffer from intrinsic low signal-to-noise ratio which is more accentuated in elastomers by the small values of dipolar couplings.

NMR images weighted by ^{1}H residual dipolar couplings as well as parameter images can be obtained for elastomers in reasonable times. By using a homogeneously cross-linked elastomer sample with a known value of the residual dipolar coupling as a reference the need for recording several images with different excitation times is avoided. The possibility of measuring parameter NMR images of ^{1}H residual dipolar couplings on static samples avoiding MAS opens up the possibility of investigating stress–strain effects in heterogeneous elastomers. Moreover, the contrast in images of residual dipolar couplings can directly be correlated with the spatial distributions of cross-link density and with viscoelastic properties. Swelling of elastomers by deuterated spy molecules which can modify the network properties is avoided.

The methods discussed above are applicable in general to partially averaged dipolar interactions and can be applied to studying segmental order in a variety of polymer networks without the need for isotopic labeling, sample rotation, or the use of cross-polarization. Proton parameter imaging of connective tissues such as cartilage and tendons with contrast from dipolar-encoded LM, DQ, and TQ filters can be envisaged to detect molecules associated with ordered structures. Work along these lines is in progress.

ACKNOWLEDGMENTS

The authors acknowledge stimulating discussions with Prof. Dr. H. W. Spiess, Prof. Dr. R. Kimmich, Dr. P. Blümler, and Dr. S. Hafner. D.E.D. thanks the Alexander von Humboldt-Stiftung for a senior research award. M.S. acknowledges the support of his contribution by DFG. The authors thank Dr. H. B. Dumler, Continental AG, Hannover, for providing the samples and for helpful information.

REFERENCES

1. F. W. Wehrli, D. Shaw, and J. B. Kneeland (Eds.), "Biomedical Magnetic Resonance Imaging: Principles, Methodology and Applications," VCH, New York (1988).
2. P. T. Callaghan, "Principles of Nuclear Magnetic Resonance Microscopy," Clarendon Press, Oxford (1991).
3. B. Blümich and W. Kuhn (Eds.), "Magnetic Resonance Microscopy," VCH, Weinheim (1992).
4. P. Blümler, B. Blümich, R. Botto, and E. Fukushima, "Spatially Resolved Magnetic Resonance," Wiley–VCH, Weinheim (1998).
5. P. Blümler and B. Blümich, *NMR: Basic Princ. Prog.* **30,** 209 (1994).
6. S. Hafner, D. E. Demco, and R. Kimmich, *Solid State NMR* **6,** 275 (1996).
7. P. Blümler and B. Blümich, *Rubber Chem. Technol.* **70,** 468 (1997).
8. P. J. McDonald, *Prog. NMR Spectrosc.* **30,** 69 (1997).
9. P. Blümler and B. Blümich, *Macromolecules* **24,** 2183 (1991).
10. A. Spyros, N. Chandarkumar, M. Heidenreich, and R. Kimmich, *Macromolecules* **31,** 3021 (1998).
11. J. A. Chudek and G. Hunter, *J. Mater. Sci. Lett.* **11,** 222 (1992).
12. S. Hafner and P. Barth, *Magn. Reson. Imaging* **5,** 739 (1995).
13. A. Spyros, R. Kimmich, B. H. Briese, and D. Jendrossek, *Macromolecules* **30,** 8278 (1997).
14. C. A. Fyfe, L. H. Randall, and N. E. Burlinson, *J. Polym. Sci. Part A: Polym. Chem.* **31,** 159 (1996).

15. S. Hafner and W. Kuhn, *Magn. Reson. Imaging* **12,** 1075 (1994).
16. S. Sarkar and R. A. Komoroski, *Macromolecules* **25,** 1420 (1992).
17. C. Chang and R. A. Komoroski, *Macromolecules* **22,** 600 (1989).
18. L. Garrido, J. E. Mark, C. C. Sun, J. L. Ackerman, and C. Chang, *Macromolecules* **24,** 4067 (1991).
19. S. R. Smith and J. L. Koenig, *Macromolecules* **24,** 3496 (1991).
20. W. Kuhn, P. Barth, S. Hafner, G. Simon, and H. Schneider, *Macromolecules* **27,** 5773 (1994).
21. P. Barth, S. Hafner, and P. Denner, *Macromolecules* **29,** 1655 (1996).
22. E. Günther, B. Blümich, and H. W. Spiess, *Macromolecules* **25,** 3315 (1992).
23. P. Blümler and B. Blümich, *Acta Polym.* **44,** 125 (1993).
24. M. Klinkenberg, P. Blümler, and B. Blümich, *Macromolecules* **30,** 1038 (1997).
25. M. Klinkenberg, P. Blümler, and B. Blümich, *J. Magn. Reson. A* **119,** 197 (1996).
26. R. Graf, D. E. Demco, S. Hafner, and H. W. Spiess, *Solid State Nucl. Magn. Reson.* **12,** 139 (1998).
27. M. Schneider, L. Gasper, D. E. Demco, and B. Blümich, *J. Chem. Phys.* **111,** 402 (1999).
28. Y. Seo, H. Takamiya, H. Ishikawa, T. Nakashima, Y. Sharf, and G. Navon, *in* "Spatially Resolved Magnetic Resonance" (P. Blümler, B. Blümich, R. Botto, and E. Fukushima, Eds.), Wiley–VCH, Weinheim (1998).
29. L. Tsoref, H. Shinar, Y. Seo, U. Eliav, and G. Navon, *Magn. Reson. Med.* **39,** 11 (1998).
30. R. R. Ernst, G. Bodenhausen, and A. Wokaun, "Principles of Nuclear Magnetic Resonance in One and Two Dimensions," Clarendon, Oxford (1987).
31. M. Munowitz and A. Pines, *Adv. Chem. Phys.* **66,** 2 (1987).
32. D. E. Demco, S. Hafner, C. Fülber, R. Graf, and H. W. Spiess, *J. Chem. Phys.* **105,** 11285 (1996).
33. R. Graf, D. E. Demco, S. Hafner, and H. W. Spiess, *J. Chem. Phys.* **106,** 885 (1997).
34. J. Gottwald, D. E. Demco, R. Graf, and H. W. Spiess, *Chem. Phys. Lett.* **243,** 314 (1995).
35. U. Friedrich, I. Schnell, D. E. Demco, and H. W. Spiess, *Chem. Phys. Lett.* **285,** 49 (1998).
36. P. Sotta, C. Fülber, D. E. Demco, B. Blümich, and H. W. Spiess, *Macromolecules* **29,** 6222 (1996).
37. J.-P. Cohen Addad, *Prog. NMR Spectrosc.* **25,** 1 (1993).
38. B. Blümich, *Concepts Magn. Reson.* **10,** 19 (1998).